
Observation of Bose-Einstein Condensation in a Dilute Atomic Vapor

Author(s): M. H. Anderson, J. R. Ensher, M. R. Matthews, C. E. Wieman and E. A. Cornell

Source: *Science*, Jul. 14, 1995, New Series, Vol. 269, No. 5221 (Jul. 14, 1995), pp. 198-201

Published by: American Association for the Advancement of Science

Stable URL: <https://www.jstor.org/stable/2888436>

REFERENCES

Linked references are available on JSTOR for this article:

https://www.jstor.org/stable/2888436?seq=1&cid=pdf-reference#references_tab_contents

You may need to log in to JSTOR to access the linked references.

JSTOR is a not-for-profit service that helps scholars, researchers, and students discover, use, and build upon a wide range of content in a trusted digital archive. We use information technology and tools to increase productivity and facilitate new forms of scholarship. For more information about JSTOR, please contact support@jstor.org.

Your use of the JSTOR archive indicates your acceptance of the Terms & Conditions of Use, available at <https://about.jstor.org/terms>



American Association for the Advancement of Science is collaborating with JSTOR to digitize, preserve and extend access to *Science*

JSTOR

Observation of Bose-Einstein Condensation in a Dilute Atomic Vapor

M. H. Anderson, J. R. Ensher, M. R. Matthews, C. E. Wieman,*
E. A. Cornell

A Bose-Einstein condensate was produced in a vapor of rubidium-87 atoms that was confined by magnetic fields and evaporatively cooled. The condensate fraction first appeared near a temperature of 170 nanokelvin and a number density of 2.5×10^{12} per cubic centimeter and could be preserved for more than 15 seconds. Three primary signatures of Bose-Einstein condensation were seen. (i) On top of a broad thermal velocity distribution, a narrow peak appeared that was centered at zero velocity. (ii) The fraction of the atoms that were in this low-velocity peak increased abruptly as the sample temperature was lowered. (iii) The peak exhibited a nonthermal, anisotropic velocity distribution expected of the minimum-energy quantum state of the magnetic trap in contrast to the isotropic, thermal velocity distribution observed in the broad uncondensed fraction.

On the microscopic quantum level, there are profound differences between fermions (particles with half integer spin) and bosons (particles with integer spin). Every statistical mechanics text discusses how these differences should affect the behavior of atomic gas samples. Thus, it is ironic that the quantum statistics of atoms has never made any observable difference to the collective macroscopic properties of real gas samples. Certainly the most striking difference is the prediction, originally by Einstein, that a gas of noninteracting bosonic atoms will, below a certain temperature, suddenly develop a macroscopic population in the lowest energy quantum mechanical state (1, 2). However, this phenomenon of Bose-Einstein condensation (BEC) requires a sample so cold that the thermal deBroglie wavelength, λ_{dB} , becomes larger than the mean spacing between particles (3). More precisely, the dimensionless phase-space density, $\rho_{\text{ps}} = n(\lambda_{\text{dB}})^3$, must be greater than 2.612 (2, 4), where n is the number density. Fulfilling this stringent requirement has eluded physicists for decades. Certain well-known physical systems do display characteristics of quantum degeneracy, in particular superfluidity in helium and superconductivity in metals. These systems exhibit counterintuitive behavior associated with macroscopic quantum states and have been the subject of extensive study. However, in these systems the bosons are so closely packed that they can be understood only as strongly interacting systems. These strong interactions have made it difficult to understand

the detailed properties of the macroscopic quantum state and allow only a small fraction of the particles to occupy the Bose condensed state. Recently, evidence of Bose condensation in a gas of excitons in a semiconductor host has been reported (5). The interactions in these systems are weak but poorly understood, and it is difficult to extract information about the exciton gas from the experimental data. Here, we report evidence of BEC in a dilute, and hence weakly interacting, atomic vapor. Because condensation at low densities is achievable only at very low temperatures, we evaporatively cooled a dilute, magnetically trapped sample to well below 170 nK.

About 15 years ago, several groups began to pursue BEC in a vapor of spin-polarized hydrogen (6). The primary motivation was that in such a dilute atomic system one might be able to produce a weakly interacting condensate state that is much closer to the original concept of Bose and Einstein and would allow the properties of the condensate to be well understood in terms of basic interatomic interactions. In the course of this work, 1000-fold increases in phase-space density have been demonstrated with the technique of evaporative cooling of a magnetically trapped hydrogen sample (7); recently, the phase-space density has approached BEC levels. Progress has been slowed, however, by the existence of inelastic interatomic collisions, which cause trap loss and heating, and by the lack of good diagnostics for the cooled samples.

The search for BEC in a dilute sample of laser-cooled alkali atoms has a somewhat shorter history. Developments in laser trapping and cooling over the past decade made it possible to increase the phase-space density of a vapor of heavy alkali atoms by more than 15 orders of magnitude. However, several processes involving the scattered pho-

tons were found to limit the achievable temperatures (8) and densities (9), so that the resulting value for ρ_{ps} was 10^5 to 10^6 times too low for BEC. We began to pursue BEC in an alkali vapor by using a hybrid approach to overcome these limitations (10, 11). This hybrid approach involves loading a laser-cooled and trapped sample into a magnetic trap where it is subsequently cooled by evaporation. This approach is particularly well suited to heavy alkali atoms because they are readily cooled and trapped with laser light, and the elastic scattering cross sections are very large (12), which facilitates evaporative cooling.

There are three other attractive features of alkali atoms for BEC. (i) By exciting the easily accessible resonance lines, one can use light scattering to sensitively characterize the density and energy of a cloud of such atoms as a function of both position and time. This technique provides significantly more detailed information about the sample than is possible from any other macroscopic quantum system. (ii) As in hydrogen, the atom-atom interactions are weak [the S-wave scattering length a_0 is about 10^{-6} cm, whereas at the required densities the interparticle spacing (x) is about 10^{-4} cm] and well understood. (iii) These interactions can be varied in a controlled manner through the choice of spin state, density, atomic and isotopic species, and the application of external fields. The primary experimental challenge to evaporatively cooling an alkali vapor to BEC has been the achievement of sufficiently high densities in the magnetic trap. The evaporative cooling can be maintained to very low temperatures only if the initial density is high enough that the atoms undergo many (~ 100) elastic collisions during the time they remain in the trap. Using a combination of techniques to enhance the density in the optical trap, and a type of magnetic trap that provides long trap holding times and tight confinement, has allowed us to evaporatively cool to BEC.

A schematic of the apparatus is shown in Fig. 1. The optical components and magnetic coils are all located outside the ultra-high-vacuum glass cell, which allows for easy access and modification. Rubidium atoms from the background vapor were optically precooled and trapped, loaded into a magnetic trap, then further cooled by evaporation. The TOP (time orbiting potential) magnetic trap (13) we used is a superposition of a large spherical quadrupole field and a small uniform transverse field that rotates at 7.5 kHz. This arrangement results in an effective average potential that is an axially symmetric, three-dimensional (3D) harmonic potential providing tight and stable confinement during evaporation. The evaporative cooling works by selectively re-

M. H. Anderson, J. R. Ensher, M. R. Matthews, C. E. Wieman, JILA, National Institute of Standards and Technology (NIST), and University of Colorado, and Department of Physics, University of Colorado, Boulder, CO 80309, USA.

E. A. Cornell, Quantum Physics Division, NIST, JILA-NIST, and University of Colorado, and Department of Physics, University of Colorado, Boulder, CO 80309, USA.

*To whom correspondence should be addressed.

leasing the higher energy atoms from the trap; the remaining atoms then rethermalize to a colder temperature.

We accomplished this release with a radio frequency (rf) magnetic field (14). Because the higher energy atoms sample the

trap regions with higher magnetic field, their spin-flip transition frequencies are shifted as a result of the Zeeman effect. We set the frequency of the rf field to selectively drive these atoms into an untrapped spin state. For optimum cooling, the rf frequency was ramped slowly downward, causing the central density and collision rate to increase and temperature to decrease. The final temperature and phase-space density of the sample depends on the final value of the rf frequency (ν_{evap}).

A typical data cycle during which atoms are cooled from 300 K to a few hundred nanokelvin is as follows: (i) For 300 s the optical forces from a magneto-optical trap (15) (MOT) collect atoms from a room temperature, $\sim 10^{-11}$ torr vapor (10) of ^{87}Rb atoms; we used a so-called dark MOT (16) to reduce the loss mechanisms of an ordinary MOT, enabling the collection of a large number (10^7) of atoms even under our unusually low pressure conditions (17). (ii) The atom cloud is then quickly compressed and cooled to 20 μK by adjustment of the field gradient and laser frequency (18). (iii) A small magnetic bias field is applied, and a short pulse of circularly polarized laser light optically pumps the magnetic moments of all the atoms so they are parallel with the magnetic field (the $F = 2$, $m_F = 2$ angular momentum state.) (19). (iv) All laser light is removed and a TOP trap is constructed in place around the atoms, the necessary quadrupole and rotating fields being turned on in 1 ms. (v) The quadrupole field component of the TOP trap is then adiabatically ramped up to its maximum value, thereby

increasing the elastic collision rate by a factor of 5.

At this point, we had about 4×10^6 atoms with a temperature of about 90 μK in the trap. The trap has an axial oscillation frequency of about 120 Hz and a cylindrically symmetric radial frequency smaller by a factor of $\sqrt{8}$. The number density, averaged over the entire cloud, is $2 \times 10^{10} \text{ cm}^{-3}$. The elastic collision rate (19) is approximately three per second, which is 200 times greater than the one per 70 s loss rate from the trap.

The sample was then evaporatively cooled for 70 s, during which time both the rf frequency and the magnitude of the rotating field were ramped down, as described (13, 20). The choice of the value of ν_{evap} for the cycle determines the depth of the rf cut and the temperature of the remaining atoms. If ν_{evap} is 3.6 MHz, the rf “scalpel” will have cut all the way into the center of the trap and no atoms will remain. At the end of the rf ramp, we allowed the sample to equilibrate for 2 s (21) and then expanded the cloud to measure the velocity distribution. For technical reasons, this expansion was done in two stages. The trap spring constants were first adiabatically reduced by a factor of 75 and then suddenly reduced to nearly zero so that the atoms essentially expanded ballistically. A field gradient remains that supports the atoms against gravity to allow longer expansion times. Although this approach provides small transverse restoring forces, these are easily taken into account in the analysis. After a 60-ms expansion, the spatial distribution of the

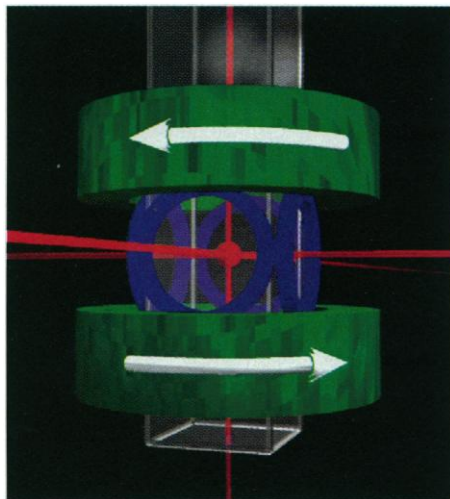


Fig. 1. Schematic of the apparatus. Six laser beams intersect in a glass cell, creating a magneto-optical trap (MOT). The cell is 2.5 cm square by 12 cm long, and the beams are 1.5 cm in diameter. The coils generating the fixed quadrupole and rotating transverse components of the TOP trap magnetic fields are shown in green and blue, respectively. The glass cell hangs down from a steel chamber (not shown) containing a vacuum pump and rubidium source. Also not shown are coils for injecting the rf magnetic field for evaporation and the additional laser beams for imaging and optically pumping the trapped atom sample.

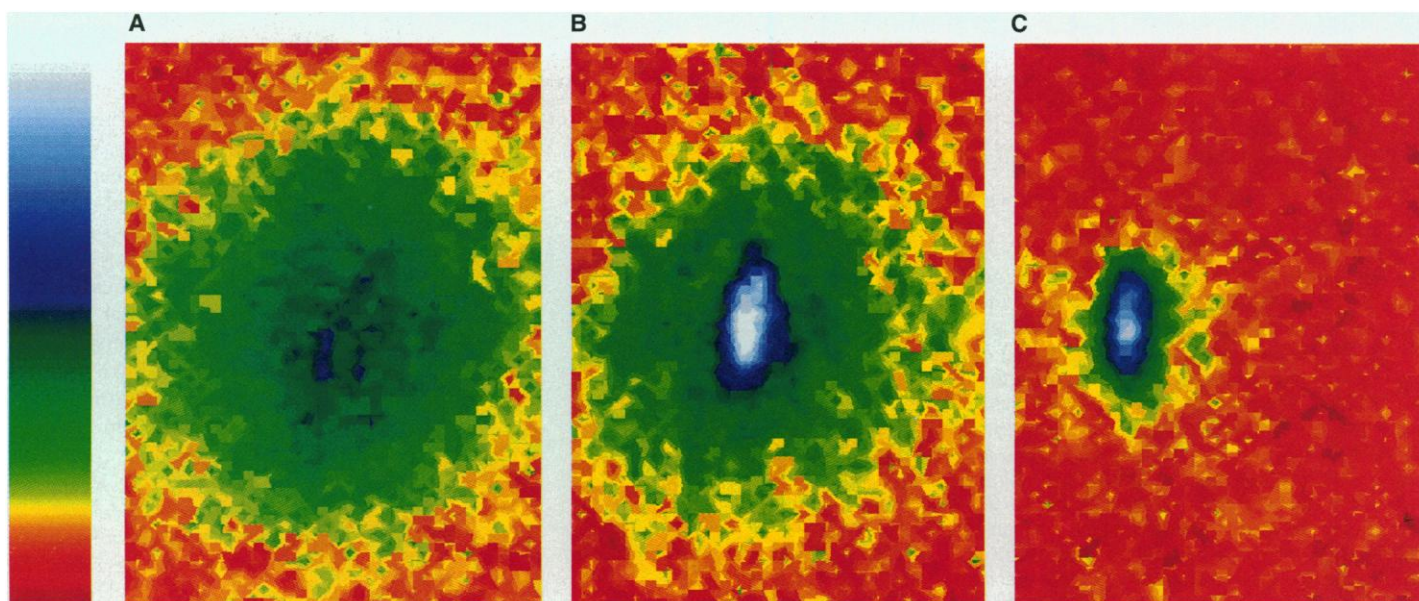


Fig. 2. False-color images display the velocity distribution of the cloud (A) just before the appearance of the condensate, (B) just after the appearance of the condensate, and (C) after further evaporation has left a sample of nearly pure condensate. The circular pattern of the noncondensate fraction (mostly yellow and green) is an indication that the velocity distribution is isotropic, consistent

with thermal equilibrium. The condensate fraction (mostly blue and white) is elliptical, indicative that it is a highly nonthermal distribution. The elliptical pattern is in fact an image of a single, macroscopically occupied quantum wave function. The field of view of each image is 200 μm by 270 μm . The observed horizontal width of the condensate is broadened by the experimental resolution.

cloud was determined from the absorption of a 20- μ s, circularly polarized laser pulse resonant with the $5S_{1/2}$, $F = 2$ to $5P_{3/2}$, $F = 3$ transition. The shadow of the cloud was imaged onto a charge-coupled device array, digitized, and stored for analysis.

This shadow image (Fig. 2) contains a large amount of easily interpreted information. Basically, we did a 2D time-of-flight measurement of the velocity distribution. At each point in the image, the optical density we observed is proportional to the column density of atoms at the corresponding part of the expanded cloud. Thus, the recorded image is the initial velocity distribution projected onto the plane of the image. For all harmonic confining potentials, including the TOP trap, the spatial distribution is identical to the velocity distribution, if each axis is linearly scaled by the harmonic oscillator frequency for that dimension (22). Thus, from the single image we obtained both the velocity and coordinate-space distributions, and from these we extracted the temperature and central density, in addi-

tion to characterizing any deviations from thermal equilibrium. The measurement process destroys the sample, but the entire load-evaporate-probe cycle can be repeated. Our data represent a sequence of evaporative cycles performed under identical conditions except for decreasing values of ν_{evap} , which gives a corresponding decrease in the sample temperature and an increase in phase-space density.

The discontinuous behavior of thermodynamic quantities or their derivatives is always a strong indication of a phase transition. In Fig. 3, we see a sharp increase in the peak density at a value of ν_{evap} of 4.23 MHz. This increase is expected at the BEC transition. As cooling proceeds below the transition temperature, atoms rapidly accumulate in the lowest energy state of the 3D harmonic trapping potential (23). For an ideal gas, this state would be as near to a singularity in velocity and coordinate space as the uncertainty principle permits.

Thus, below the transition we expect a two-component cloud, with a dense central condensate surrounded by a diffuse, noncondensate fraction. This behavior is clearly displayed in sections taken horizontally through the center of the distributions, as shown in Fig. 4. For values of ν_{evap} above 4.23 MHz, the sections show a single, smooth, Gaussian-like distribution. At 4.23 MHz, a sharp central peak in the distribution begins to appear. At frequencies below 4.23 MHz, two distinct components to the cloud are visible, the smooth broad curve and a narrow central peak, which we identify as the noncondensate and condensate

fractions, respectively. (Figs. 2B and 4). As the cooling progresses (Fig. 4), the noncondensate fraction is reduced until, at a value of ν_{evap} of 4.1 MHz, little remains but a pure condensate containing 2000 atoms.

The condensate first appears at an rf frequency between 4.25 and 4.23 MHz. The 4.25 MHz cloud is a sample of 2×10^4 atoms at a number density of $2.6 \times 10^{12} \text{ cm}^{-3}$ and a temperature of 170 nK. This represents a phase-space density ρ_{ps} of 0.3, which is well below the expected value of 2.612. The phase-space density scales as the sixth power of the linear size of the cloud. Thus, modest errors in our size calibration could explain much of this difference. Below the transition, one can estimate an effective phase-space density by simply dividing the number of atoms by the observed volume they occupy in coordinate and velocity space. The result is several hundred, which is much greater than 2.6 and is consistent with a large occupation number of a single state. The temperatures and densities quoted here were calculated for the sample in the unexpanded trap. However, after the adiabatic expansion stage, the atoms are still in good thermal equilibrium, but the temperatures and densities are greatly reduced. The 170 nK temperature is reduced to 20 nK, and the number density is reduced from $2.6 \times 10^{12} \text{ cm}^{-3}$ to $1 \times 10^{11} \text{ cm}^{-3}$. There is no obstacle to adiabatically cooling and expanding the cloud further when it is desirable to reduce the atom-atom interactions, as discussed below (24).

A striking feature evident in the images shown in Fig. 2 is the differing axial-to-radial aspect ratios for the two components of the cloud. In the clouds with no condensate ($\nu_{\text{evap}} > 4.23 \text{ MHz}$) and in the noncondensate fraction of the colder clouds, the velocity distribution is isotropic (as evidenced by the circular shape of the yellow to green contour lines in Fig. 2, A and B). But the condensate fraction clearly has a larger velocity spread in the axial direction than in the radial direction (Fig. 2, B and C). This difference in aspect ratios is readily explained and in fact is strong evidence in support of the interpretation that the central peak is a Bose-Einstein condensate. The noncondensate atoms represent a thermal distribution across many quantum wave functions. In thermal equilibrium, velocity distributions of a gas are always isotropic regardless of the shape of the confining potential. The condensate atoms, however, are all described by the same wave function, which will have an anisotropy reflecting that of the confining potential. The velocity spread of the ground-state wave function for a noninteracting Bose gas should be 1.7 ($8^{1/4}$) times larger in the axial direction than in the radial direction. Our observations are in qualitative agreement with this

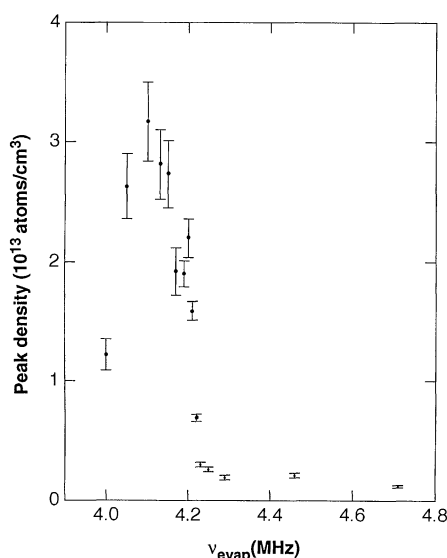


Fig. 3. Peak density at the center of the sample as a function of the final depth of the evaporative cut, ν_{evap} . As evaporation progresses to smaller values of ν_{evap} , the cloud shrinks and cools, causing a modest increase in peak density until ν_{evap} reaches 4.23 MHz. The discontinuity at 4.23 MHz indicates the first appearance of the high-density condensate fraction as the cloud undergoes a phase transition. When a value for ν_{evap} of 4.1 MHz is reached, nearly all the remaining atoms are in the condensate fraction. Below 4.1 MHz, the central density decreases, as the evaporative "rf scalpel" begins to cut into the condensate itself. Each data point is the average of several evaporative cycles, and the error bars shown reflect only the scatter in the data. The temperature of the cloud is a complicated but monotonic function of ν_{evap} . At $\nu_{\text{evap}} = 4.7 \text{ MHz}$, $T = 1.6 \mu\text{K}$, and for $\nu_{\text{evap}} = 4.25 \text{ MHz}$, $T = 180 \text{ nK}$.

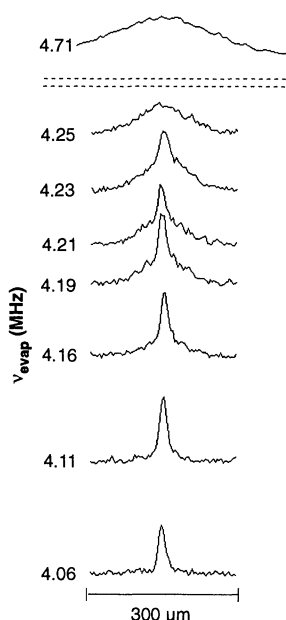


Fig. 4. Horizontal sections taken through the velocity distribution at progressively lower values of ν_{evap} show the appearance of the condensate fraction.

simple picture. This anisotropy rules out the possibility that the narrow peak we see is a result of the enhanced population of all the very low energy quantum states, rather than the single lowest state.

A more quantitative treatment of the observed shape of the condensate shows that the noninteracting gas picture is not completely adequate. We find that the axial width is about a factor of 2 larger than that calculated for a noninteracting ground state and the ratio of the axial to radial velocity spread is at least 50% larger than calculated. However, the real condensate has a self-interaction energy in the mean-field picture of $4\pi n a_0 \hbar^2/m$, which is comparable to the separation between energy levels in the trap. Simple energy arguments indicate that this interaction energy will tend to increase both the size and the aspect ratio to values more in line with what we observed.

Although an atomic vapor of rubidium can only exist as a metastable state at these temperatures, the condensate survives in the unexpanded trap for about 15 s, which is long enough to carry out a wide variety of experiments. The loss rate is probably a result of three-body recombination (25, 26), which could be greatly reduced by adiabatically expanding the condensate after it has formed.

Much of the appeal of our work is that it permits quantitative calculations of microscopic behavior, heuristic understanding of macroscopic behavior, and experimental verification of both. The technique and apparatus described here are well suited for a range of experiments. The basic glass cell design provides flexibility in manipulating and probing the atoms. In addition, it is not difficult to substantially improve it in several ways. First, our position and velocity resolution can be improved with minor changes in optics and in expansion procedures. Second, a double MOT technique that spatially separates the capture and storage of atoms will increase our number of atoms by more than 100 (27). Third, with improvement in measurement sensitivity it should be possible to probe the cloud without destroying it, in order to watch the dynamics in real time.

An abbreviated list of future experiments includes (i) performing optical spectroscopy, including higher order correlation measurements, on the condensate in situ to study how light interacts differently with coherent matter and incoherent matter (28); (ii) comparing the behaviors of ^{87}Rb with ^{85}Rb , which is known to have a negative scattering length (19), potentially making the condensate unstable; (iii) studying time-dependent behavior of the phase transition including the

stability of the supersaturated state; (iv) exploring the specific heat of the sample as it goes through the transition boundary (2) by measuring how condensate and noncondensate fractions evolve during cooling; (v) studying critical opalescence and other fluctuation-driven behavior near the transition temperature; and (vi) carrying out experiments analogous to many of the classic experiments on superfluid helium (2, 29). There is a prediction that the scattering length of heavy alkalis can be modified, and even be made to change sign, by tuning the ambient magnetic field through a scattering resonance (26). Directly modifying the scattering length would provide the ultimate control, but whether or not this is practical, one can still study the properties of the condensate as functions of the strength of the residual interactions because we now have the ability to cross the phase-transition curve over a large range of densities. Thus, it will be possible to observe, and to compare with theoretical prediction, the emergence of nonideal behavior such as singularities in the specific heat and many other phenomena, including those mentioned above.

REFERENCES AND NOTES

1. S. N. Bose, *Z. Phys.* **26**, 178 (1924); A. Einstein, *Sitzungsber. Kgl. Preuss. Akad. Wiss.* **1924**, 261 (1924); *ibid.* **1925**, 3 (1925); A. Griffin, D. W. Snoke, A. Stringari, Eds., *Bose Einstein Condensation* (Cambridge Univ. Press, Cambridge, 1995).
2. K. Huang, *Statistical Mechanics 2nd Edition* (Wiley, New York, 1987).
3. $\lambda_{\text{dB}} = h/(2\pi mkT)^{1/2}$, where h is Planck's constant, m is the mass of the atom, k is Boltzmann's constant, and T is the temperature.
4. V. Bagnato, D. E. Pritchard, D. Kleppner, *Phys. Rev. A* **35**, 4354 (1987).
5. J.-L. Lin and J. P. Wolfe, *Phys. Rev. Lett.* **71**, 1222 (1993).
6. For reviews of the hydrogen work, see T. J. Greytak and D. Kleppner, in *New Trends in Atomic Physics, Proceedings of the Les Houches Summer School, Session XXXVIII*, Les Houches, France, 2 to 28 June 1993, G. Greenberg and R. Stora, Eds. (North-Holland, Amsterdam, Netherlands, 1984), pp. 1127–1158; I. F. Silvera and J. T. M. Walraven, in *Progress in Low Temperature Physics*, D. Brewer, Ed. (North-Holland, Amsterdam, Netherlands, 1986), vol. 10, pp. 139–173; T. J. Greytak, in *Bose Einstein Condensation*, A. Griffin, D. W. Snoke, A. Stringari, Eds. (Cambridge Univ. Press, Cambridge, 1995), pp. 131–159.
7. N. Masuhara *et al.*, *Phys. Rev. Lett.* **61**, 935 (1988); O. J. Luiten *et al.*, *ibid.* **70**, 544 (1993); H. F. Hess, *Phys. Rev. B* **34**, 3476 (1986).
8. C. Wieman and S. Chu, Eds., *J. Opt. Soc. Am. B* **6** (no. 11) (1989) (special issue on laser cooling and trapping of atoms; in particular, see the "Optical Molasses" section).
9. D. Sesko, T. Walker, C. Monroe, A. Gallagher, C. Wieman, *Phys. Rev. Lett.* **63**, 961 (1989); T. Walker, D. Sesko, C. Wieman, *ibid.* **64**, 408 (1990); D. Sesko, T. Walker, C. Wieman, *J. Opt. Soc. Am. B* **8**, 946 (1991).
10. C. Monroe, W. Swann, H. Robinson, C. Wieman, *Phys. Rev. Lett.* **65**, 1571 (1990).
11. C. Monroe, E. Cornell, C. Wieman, in proceedings of the Enrico Fermi International Summer School on Laser Manipulation of Atoms and Ions, Varenna, Italy, 7 to 21 July 1991, E. Arimondo, W. Phillips, F. Strumia, Eds. (North-Holland, Amsterdam, Netherlands, 1992), pp. 361–377.
12. C. Monroe, E. Cornell, C. Sackett, C. Myatt, C. Wieman, *Phys. Rev. Lett.* **70**, 414 (1993); N. Newbury, C. Myatt, C. Wieman, *Phys. Rev. A* **51**, R2680 (1995).
13. W. Petrich, M. H. Anderson, J. R. Ensher, E. A. Cornell, *Phys. Rev. Lett.* **74**, 3352 (1995).
14. D. Pritchard *et al.*, in *Proceedings of the 11th International Conference on Atomic Physics*, S. Haroche, J. C. Gay, G. Grynberg, Eds. (World Scientific, Singapore, 1989), pp. 619–621. The orbiting zero-field point in the TOP trap supplements the effect of the rf by removing some high-energy atoms by Majorana transitions. Two other groups have evaporatively cooled alkali atoms [C. S. Adams, H. J. Lee, N. Davidson, M. Kasevich, S. Chu, *Phys. Rev. Lett.* **74**, 3577 (1995); K. B. Davis, M.-O. Mewes, M. A. Joffe, M. R. Andres, W. Ketterle, *ibid.*, p. 5202].
15. E. Raab, M. Prentiss, A. Cable, S. Chu, D. E. Pritchard, *Phys. Rev. Lett.* **59**, 2631 (1987).
16. W. Ketterle, K. B. Davis, M. A. Joffe, A. Martin, D. E. Pritchard, *ibid.* **70**, 2253 (1993).
17. M. H. Anderson, W. Petrich, J. R. Ensher, E. A. Cornell, *Phys. Rev. A* **50**, R3597 (1994).
18. W. Petrich, M. H. Anderson, J. R. Ensher, E. A. Cornell, *J. Opt. Soc. Am. B* **11**, 1332 (1994).
19. J. R. Gardner *et al.* [*Phys. Rev. Lett.* **74**, 3764 (1995)] determined the ground-state triplet scattering lengths and found that they are positive for ^{87}Rb and negative for ^{85}Rb . It is believed that a positive scattering length is necessary for the stability of large samples of condensate. The $F = 2, m_F = 2$ state also has the advantage that, of the Rb 5S states, it is the spin state with the maximum magnetic trapping force.
20. After the rotating field has been reduced to one-third its initial value, which increases the spring constant by a factor of 3, it is held fixed (at 5 G) and the final cooling is done only with the rf ramp.
21. After the sample is cooled to just below the transition temperature, the condensate peak does not appear immediately after the ramp ends but instead grows during this 2-s delay.
22. This exact correspondence between velocity and coordinate-space distributions requires that the particles be an ideal gas, which is an excellent approximation in our system, except in the condensate itself. It also requires that sinusoidal trajectories of the atoms have random initial phase. This is much less restrictive than requiring thermal equilibrium.
23. Below the transition temperature the fraction of the atoms that go into the condensate is basically set by the requirement that the phase-space density of the noncondensate fraction not exceed 2.612 (for an ideal gas). As the cloud is further cooled or compressed, the excess atoms are squeezed into the condensate (2).
24. The temperature of a classical gas that would correspond to the kinetic energy of the pure condensate cloud ($\nu_{\text{evap}} = 4.11$ MHz), after adiabatic expansion, is only 2 nK, and during the near-ballistic expansion it becomes substantially lower.
25. E. Tiesinga, A. J. Moerdijk, B. J. Verhaar, H. T. C. Stoof, *Phys. Rev. A* **46**, R1167 (1992).
26. E. Tiesinga, B. J. Verhaar, H. T. C. Stoof, *ibid.* **47**, 4114 (1993).
27. C. Myatt, N. Newbury, C. Wieman, personal communication.
28. L. You, M. Lewenstein, J. Cooper, *Phys. Rev. A* **51**, 4712 (1995) and references therein; O. Morice, Y. Castin, J. Dalibard, *ibid.*, p. 3896; J. Javanainen, *Phys. Rev. Lett.* **72**, 2375 (1994); B. V. Svistunov and G. V. Shlyapnikov, *JETP* **71**, 71 (1990).
29. P. A. Ruprecht, M. J. Holland, K. Burnett, M. Edwards, *Phys. Rev. A* **51**, 4704 (1995).
30. During the adiabatic stage of expansion, we already routinely changed the sample density by a factor of 25.
31. We thank K. Coakley, J. Cooper, M. Dowell, J. Doyle, S. Gilbert, C. Greene, M. Holland, D. Kleppner, C. Myatt, N. Newbury, W. Petrich, and B. Verhaar for valuable discussions. This work was supported by National Science Foundation, National Institute of Standards and Technology, and the Office of Naval Research.

26 June 1995; accepted 29 June 1995